

# A 2 Magnetism in Density Functional Theory

G. Bihlmayer

Institut für Festkörperforschung

Forschungszentrum Jülich GmbH

## Contents

<b>1</b>	<b>Density Functional Theory</b>	<b>2</b>
1.1	The density and potential matrix . . . . .	2
1.2	The collinear case . . . . .	4
1.3	Orbital magnetism . . . . .	5
<b>2</b>	<b>The magnetic ground state</b>	<b>6</b>
2.1	Spin-dynamics, magnetic torque . . . . .	7
2.2	Constrained DFT . . . . .	9
2.3	Mapping on model Hamiltonians . . . . .	10
<b>3</b>	<b>Beyond the ground state</b>	<b>11</b>
3.1	Low temperatures: magnons and spin waves . . . . .	11
3.2	Spin-spirals and the generalized Bloch theorem . . . . .	13
3.3	High temperatures: $T_C$ and $T_N$ . . . . .	14

# 1 Density Functional Theory

In 1964 Hohenberg and Kohn [1] worked out two central theorems that form the basis of density functional theory (DFT): For a system of  $N$  particles (e.g. electrons) moving in an external potential  $v(\mathbf{r})$  (caused by e.g. nuclei) in a non-degenerate ground state (i) the many-body wavefunction  $\Psi$  and  $v(\mathbf{r})$  are uniquely determined by the particle density distribution  $n(\mathbf{r})$  and (ii) there exists an energy functional of this density,  $E[n(\mathbf{r})]$ , which is stationary with respect to variations of the ground-state density. These two theorems allow – at least in principle – the determination of the ground-state density and energy of an  $N$ -particle system. Extracting the classical Coulomb interaction energy, such a Hohenberg-Kohn energy functional takes the form

$$E[n(\mathbf{r})] = \int v(\mathbf{r})n(\mathbf{r})d\mathbf{r} + \frac{1}{2} \iint \frac{n(\mathbf{r})n(\mathbf{r}')}{|\mathbf{r} - \mathbf{r}'|} d\mathbf{r}d\mathbf{r}' + G[n(\mathbf{r})] \quad (1)$$

where the functional  $G[n(\mathbf{r})]$  has to be approximated.

In the Kohn-Sham theory [2], the kinetic energy  $T_0$  of a non-interacting electron gas in its ground state with a density distribution  $n(\mathbf{r})$  is further extracted from  $G[n(\mathbf{r})]$ , so that a new functional

$$E_{xc}[n(\mathbf{r})] = G[n(\mathbf{r})] - T_0[n(\mathbf{r})] \quad (2)$$

remains to be determined.  $E_{xc}$  is now called exchange-correlation energy functional, since without  $E_{xc}$  our energy functional  $E$  would yield just the Hartree energy. If we take into account that particle conservation, i.e.  $N = \int n(\mathbf{r})d\mathbf{r}$  has to be ensured, we can formulate the stationarity of  $E$  in Eq. (1) with respect to variations of the ground-state density as

$$v(\mathbf{r}) + \int \frac{n(\mathbf{r}')}{|\mathbf{r} - \mathbf{r}'|} d\mathbf{r}' + \frac{\delta T_0}{\delta n(\mathbf{r})} + \frac{\delta E_{xc}}{\delta n(\mathbf{r})} - \lambda = 0 \quad (3)$$

where the Lagrange parameter  $\lambda$  ensures the particle conservation. Expressing the kinetic energy of the non-interacting particles via their wavefunctions,  $\phi_i$ , we can recast Eq. (3) in the form of an effective single particle Schrödinger equation:

$$\left[ -\frac{\hbar^2}{2m} \nabla^2 + v(\mathbf{r}) + \int \frac{n(\mathbf{r}')}{|\mathbf{r} - \mathbf{r}'|} d\mathbf{r}' + \frac{\delta E_{xc}}{\delta n(\mathbf{r})} \right] \phi_i(\mathbf{r}) = \epsilon_i \phi_i(\mathbf{r}) \quad (4)$$

which has to be solved self-consistently since  $n(\mathbf{r}) = \sum_{i=1}^N |\phi_i(\mathbf{r})|^2$ . The last term of the Hamiltonian is called the exchange-correlation potential.

## 1.1 The density and potential matrix

In 1972 von Barth and Hedin extended this concept to spin-polarized systems [3], replacing the scalar density by a hermitian  $2 \times 2$  matrix  $\underline{n}(\mathbf{r})$ . If  $\psi_\alpha(\mathbf{r})$  is the field operator for a particle of spin  $\alpha$ , a component of the spin-density matrix can be defined as

$$n_{\alpha\beta}(\mathbf{r}) = \langle \Psi | \psi_\beta^\dagger(\mathbf{r}) \psi_\alpha(\mathbf{r}) | \Psi \rangle. \quad (5)$$

The potential matrix corresponding to this spin-density matrix is denoted as  $\underline{v}(\mathbf{r})$  and replaces the scalar potential. Then, we can write Eq. (4) in the form

$$\left[ \left( -\frac{\hbar^2}{2m} \nabla^2 + \sum_\alpha \int \frac{n_{\alpha\alpha}(\mathbf{r}')}{|\mathbf{r} - \mathbf{r}'|} d\mathbf{r}' \right) \mathbb{I} + \underline{v}(\mathbf{r}) + \frac{\delta E_{xc}}{\delta \underline{n}(\mathbf{r})} \right] \begin{pmatrix} \phi_i^{(+)}(\mathbf{r}) \\ \phi_i^{(-)}(\mathbf{r}) \end{pmatrix} = \epsilon_i \begin{pmatrix} \phi_i^{(+)}(\mathbf{r}) \\ \phi_i^{(-)}(\mathbf{r}) \end{pmatrix} \quad (6)$$

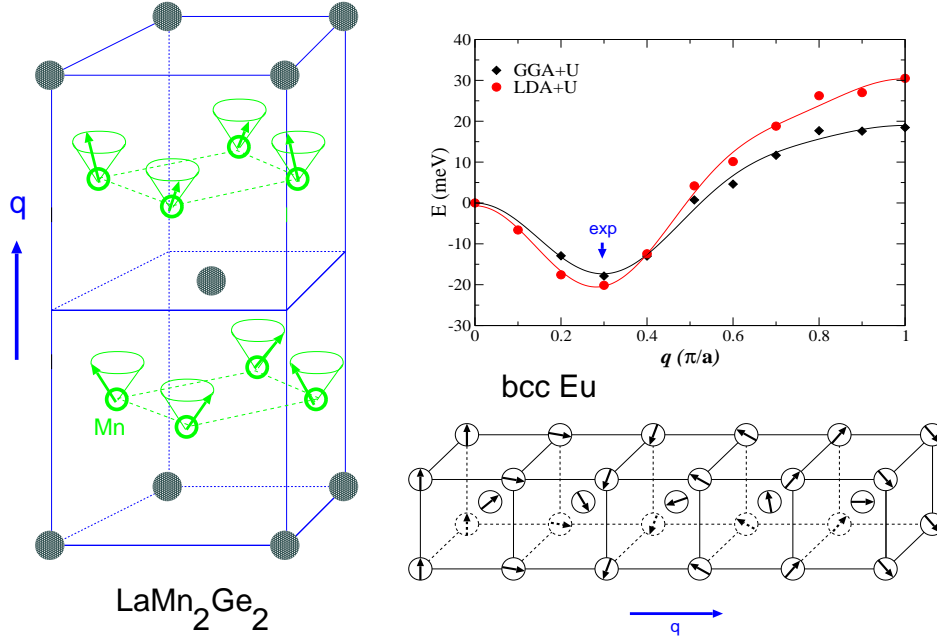


**Fig. 1:** Examples of non-collinear ground-states: in  $\text{LaMn}_2\text{Ge}_2$  the spins on the Mn sublattice can be described by a conical spin-spiral, i.e. the magnetization precesses on a cone with a semicone-angle of  $58^\circ$  from layer to layer in  $z$ -direction. The turning angle per layer is  $128^\circ$ . The magnetic structure is in good agreement with first-principles calculations [4]. Bulk bcc europium has a flat spiral in  $[001]$  direction as ground state (right, bottom), the length of the  $\mathbf{q}$ -vector, describing this precession, is correctly reproduced in DFT calculations [5] (right, top).

where  $\underline{\mathbb{I}}$  is a  $2 \times 2$  unit matrix and the exchange-correlation potential is now also a  $2 \times 2$  matrix. In terms of the Kohn-Sham wavefunctions, the density matrix can now be written as

$$n_{\alpha\beta}(\mathbf{r}) = \sum_{i=1}^N \phi_i^{*\alpha}(\mathbf{r}) \phi_i^\beta(\mathbf{r}) \quad \text{where} \quad \alpha, \beta = (+), (-). \quad (7)$$

Using the Pauli matrices,  $\underline{\sigma}$ , the density matrix can be decomposed in a scalar and a vectorial part, corresponding to the charge and magnetization density:

$$\underline{n}(\mathbf{r}) = \frac{1}{2} (n(\mathbf{r})\underline{\mathbb{I}} + \underline{\sigma} \cdot \mathbf{m}(\mathbf{r})) = \frac{1}{2} \begin{pmatrix} n(\mathbf{r}) + m_z(\mathbf{r}) & m_x(\mathbf{r}) - im_y(\mathbf{r}) \\ m_x(\mathbf{r}) + im_y(\mathbf{r}) & n(\mathbf{r}) - m_z(\mathbf{r}) \end{pmatrix}. \quad (8)$$

Likewise, the potential matrices can be written in terms of a scalar potential and magnetic field,  $\mathbf{B}(\mathbf{r})$ :

$$\underline{v}(\mathbf{r}) = v(\mathbf{r})\underline{\mathbb{I}} + \mu_B \underline{\sigma} \cdot \mathbf{B}(\mathbf{r}) \quad \text{and} \quad \underline{v}_{\text{xc}}(\mathbf{r}) = v_{\text{xc}}(\mathbf{r})\underline{\mathbb{I}} + \mu_B \underline{\sigma} \cdot \mathbf{B}_{\text{xc}}(\mathbf{r}) \quad (9)$$

where  $\mu_B = \frac{e\hbar}{2mc}$  is the Bohr magneton.

Within this formalism, general non-collinear structures can be described in the framework of density functional theory. Two recent examples,  $\text{LaMn}_2\text{Ge}_2$  and bcc-Eu, are shown in Fig. 1. Numerically, Eq. (6) is solved by expanding  $\phi_i(\mathbf{r})$  in a linear combination of suitable basis-functions  $\chi_j(\mathbf{r})$ . Then Eq. (6) transforms into an eigenvalue problem and the eigenvectors,

that have to be determined, give the linear combination coefficients,  $c_{ij}$ , of the expansion  $\phi_i(\mathbf{r}) = \sum_j c_{ij} \chi_j(\mathbf{r})$ . Such an eigenvalue problem is a standard problem of linear algebra and the computational effort scales in the most general case with the third power of the number of basis-functions. Compared to the non-magnetic problem, Eq. (4), this number is doubled in Eq. (6). Therefore, the computational effort for a general, non-collinear calculation is increased by a factor eight as compared to the non-magnetic calculation.

## 1.2 The collinear case

Supposing that the potential matrices in Eq. (9) are diagonal (i.e. the magnetic and exchange fields point in  $z$  direction), Eq. (6) decouples into two equations of the type of Eq. (4):

$$\begin{aligned} \left( -\frac{\hbar^2}{2m} \nabla^2 + v_{\text{Coul}}(\mathbf{r}) + v(\mathbf{r}) + B_z(\mathbf{r}) + v_{\text{xc}}^{(+)}(\mathbf{r}) \right) \phi_i^{(+)}(\mathbf{r}) &= \epsilon_i^{(+)} \phi_i^{(+)}(\mathbf{r}) \\ \left( -\frac{\hbar^2}{2m} \nabla^2 + v_{\text{Coul}}(\mathbf{r}) + v(\mathbf{r}) - B_z(\mathbf{r}) + v_{\text{xc}}^{(-)}(\mathbf{r}) \right) \phi_i^{(-)}(\mathbf{r}) &= \epsilon_i^{(-)} \phi_i^{(-)}(\mathbf{r}) \end{aligned} \quad (10)$$

where  $v_{\text{Coul}}$  denotes now the classical Coulomb potential and  $v_{\text{xc}}^{(+,-)}$  the exchange-correlation potential that arises from the functional derivative of the exchange-correlation energy with respect to the spin-up (+) or spin-down (−) part of the diagonal density matrix.

Since the two equations (10) can be solved independently, the computational effort for a collinear calculation seems to be just twice the effort for a non-magnetic calculation. However, most magnetic calculations are computationally considerably more demanding since the quantities in question (magnetic moments, energy differences between various magnetic configurations) require much higher accuracy than what is needed for nonmagnetic systems. To explore different magnetic orders in a system, unit cells much larger than the chemical unit cell are required, e.g. antiferromagnetic body-centered cubic (bcc) chromium requires a calculation with at least two atoms in the unit cell (as compared to one, in a nonmagnetic calculation).

Systems that can be described by Eq. (10) are all kinds of magnetic materials that assume a collinear magnetic order, e.g. ferromagnetic, antiferromagnetic or ferrimagnetic states. Like the density, that can – at least in principle – be obtained exactly in DFT, the spin density is a property that is well defined in spin-polarized DFT:

$$\mathbf{m}(\mathbf{r}) = -\mu_B \sum_{\alpha,\beta} \psi_{\alpha}^{\dagger}(\mathbf{r}) \boldsymbol{\sigma}_{\alpha\beta} \psi_{\beta}(\mathbf{r}). \quad (11)$$

The integral spin moment,  $M$ , for a collinear system is then (in units of  $\mu_B$ ) simply

$$M_{\text{spin}} = \int \mathbf{m}(\mathbf{r}) d\mathbf{r} = \int (n^{(+)}(\mathbf{r}) - n^{(-)}(\mathbf{r})) d\mathbf{r}. \quad (12)$$

How well this quantity corresponds to experimental values depends of course on the quality of the exchange-correlation potential that is used for an actual calculation. Some examples of results obtained in the local spin density approximation (LSDA) and generalized gradient approximation (GGA) of (spin)-moments of elemental ferromagnets are given in table 1.

The success of DFT calculations for magnetic systems – as shown in table 1 – has to be contrasted here with the case of Cr, where up to now no satisfactory agreement with experimental results was obtained: while LSDA calculations of antiferromagnetic Cr at the experimental lattice constant give a magnetic moment in nice agreement with experimental data ( $0.5 - 0.6 \mu_B$ ),

**Table 1:** Magnetic moments (in  $\mu_B$  per atom) of ferromagnetic elements in the bulk. The experimentally determined total magnetization,  $M_{\text{tot.}}$ , consists of spin- and orbital moment contributions. The LSDA results for Fe, Co and Ni are taken from Moruzzi et al. [6], the GGA values from Shallcross and coworkers [7] where also experimental values are quoted. The calculated Gd data is from Kurz et al. [8], the experimental one from White and coworkers [9].

Property	source	Fe (bcc)	Co (fcc)	Ni (fcc)	Gd (hcp)
$M_{\text{spin}}$	LSDA	2.15	1.56	0.59	7.63
$M_{\text{spin}}$	GGA	2.22	1.62	0.62	7.65
$M_{\text{spin}}$	experiment	2.12	1.57	0.55	
$M_{\text{tot.}}$	experiment	2.22	1.71	0.61	7.63

calculations at the lattice constant determined with LSDA (which is 3% too small) yield a non-magnetic ground state. GGA calculations, on the other hand, give a reasonable lattice constant but the magnetic moment is more than 60% too large [10]. Also attempts to include the experimentally observed incommensurate sinusoidal modulation of the antiferromagnetic structure of Cr could nor resolve these discrepancies so far.

At this point we should notice, that we relied on the assumption that the total energy is invariant with respect to a uniform rotation of the magnetization direction. This was implicitly assumed when we arbitrarily (or, better, for convenience) selected in Eq. (10) the  $z$  direction as global magnetization axis. Indeed, in absence of an external field (or in its presence, as long as it is oriented in  $z$  direction) this implies no loss in generality, if  $v_{\text{xc}}$  is isotropic in space. If we start from a Schrödinger-Pauli like theory, there is indeed no term that could couple the spin-space to the lattice. Only if a spin-orbit coupling term (from a Dirac type theory) or – in some cases – dipolar interaction is included, a preferential direction for the collinear magnetization exists. This will be discussed in the next section.

### 1.3 Orbital magnetism

The magnetization density we discussed in the last section, Eq. (11), is clearly a consequence of the imbalance of electrons with spin-up or spin-down and, therefore, the quantity defined in Eq. (12) is called spin-moment. From atomic physics we know, that the total magnetic moment is a sum of spin- and orbital contributions,  $M_{\text{tot.}} = M_{\text{spin}} + M_{\text{orb.}}$ . The orbital moment results, in a classical picture, from the orbital motion of the electron around the nucleus. Compared to the situation in a free atom, where  $M_{\text{orb}}$  can be even larger than  $M_{\text{spin}}$ , in a solid this motion is of course restricted by the crystal field that quenches the orbital moment. In bulk samples small moments (typically  $0.1 - 0.2\mu_B$ ) can be found (compare table 1).

Density functional theory in the known LSDA or GGA formulations provides no term that could lead to the formation of an orbital moment. Current- and spin-density functional theory [11] would provide a natural starting point for the description of orbital magnetism, but so far the successes are limited. From relativistic quantum mechanics [12], a two-component approximation to the Dirac equation can be formulated, that has the form of Eq. (6). From the several terms appearing in this Pauli equation one term, the spin-orbit coupling term, provides a mechanism that leads to orbital polarization: The electron, traveling on a classical trajectory around the nucleus, experiences the electric field (from the screened nucleus) as a magnetic field. This

field couples to the magnetic (spin) moment of the electron and, thus, leads to a preferential orientation of the orbital motion. Using the orbital moment operator  $\mathbf{L} = \mathbf{r} \times \mathbf{v}$ , we can write the spin-orbit coupling term in the vicinity of a nucleus with a radial potential  $v(r)$  as:

$$H_{\text{so}} = \frac{1}{r} \frac{dv(r)}{dr} (\boldsymbol{\sigma} \cdot \mathbf{L}). \quad (13)$$

Adding this term to Eq. (6) will destroy a decoupling of spin-up and -down equations like in Eq. (10). It also invalidates the aforementioned assumption that the total energy is not affected by a uniform rotation of the spin directions, since now spin-space and lattice are coupled by Eq. (13).

The orbital magnetization can be defined in analogy to Eq. (11), expressed in single particle wavefunctions  $\phi_i$ :

$$\mathbf{m}(\mathbf{r}) = -\mu_B \sum_i \langle \phi_i | \mathbf{r} \times \mathbf{v} | \phi_i \rangle. \quad (14)$$

At a certain atom  $\nu$ , the orbital moment  $M_\nu^{\text{orb}}$  can then be obtained by an integration in a sphere centered around this atom:

$$M_\nu^{\text{orb}} = -\mu_B \sum_i \langle \phi_i | \mathbf{L} | \phi_i \rangle_\nu. \quad (15)$$

While this definition of the orbital moment poses no difficulties in periodic solids, we note here that the evaluation of the total orbital moment of a periodic crystal is more involved [13]. In most cases, however, the atomic orbital moments and also the magnetic anisotropy energies, obtained in density functional theory calculations, are too small as compared to experiment. Practical methods that can overcome this deficiency have been discussed in the literature [14]. Since the crystal field in a solid forces the orbital motion of the electron in a preferred plane, a total energy difference arises when the solid is magnetized in two different directions [15]. This difference, magnetocrystalline anisotropy energy (MAE), is small for bulk systems with high symmetry, e.g. cubic crystals like Fe or Ni. It is larger for crystals with a unique crystallographic axis, like hexagonal Co. But for lower dimensional systems, thin films or atomic wires, the magnetocrystalline anisotropy will essentially determine the magnetic properties, especially at finite temperatures [16].

The computational effort for calculations that include the spin-orbit coupling term, Eq. (13), can be reduced if this term is considered as a small perturbation to the non-relativistic Schrödinger-Pauli Hamiltonian. Then, the so-called magnetic force theorem [17] can be used to evaluate quantities like the MAE. But even these calculations require considerable computational resources, since the energy differences to be determined are very small and – compared to normal calculations – drastically increased numerical cutoffs can be necessary. Systems, where spin-orbit coupling is strong require a self-consistent treatment including Eq. (13) in the Hamiltonian. There, of course, the relativistic effects are stronger so that moderate numerical cutoffs can be used, but the computational complexity brought by the spin-orbit coupling term and the loss of symmetry still leads to an increased computational effort.

## 2 The magnetic ground state

To determine the magnetic ground state it is possible to follow several directions: like in molecular-dynamics calculations, spin-dynamics allows to study the magnetic degrees of freedom exploring the ground state configuration. Another possibility is to determine the magnetic

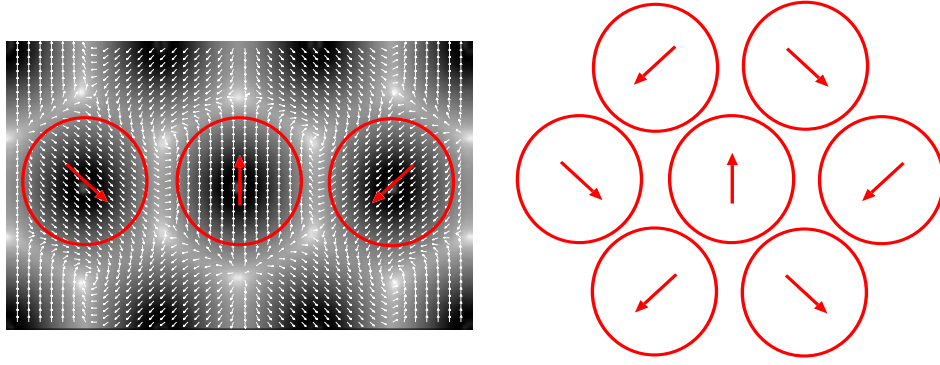


**Fig. 2:** Left: ground state magnetization density of a hexagonal Cr monolayer with the Cu(111) in-plane lattice constant; the absolute value of the magnetization is shown in greyscale, the local directions are marked by small arrows. The average magnetization direction around an atom is indicated as red arrows. Right: schematic picture of the magnetic structure (Néel state) of the hexagonal Cr monolayer.

interactions between the atoms by a DFT calculation which are then mapped onto a model (in the simplest case a classical Heisenberg model). This model is then solved, either analytically or numerically. In both cases we introduce a discretization of the (vector) magnetization density: In spin-dynamics, the evolution of discrete spins, i.e. vectors attached to certain (atomic) positions is monitored. Also mapping the *ab-initio* results to a model Hamiltonian which contains interactions between spins requires that it is possible to assign a definite spin to an atom, so that it should be possible to write in the vicinity of an atom  $\nu$ , e.g. within some sphere centered at the nucleus, the magnetization density,  $\mathbf{m}(\mathbf{r})$ , as

$$\mathbf{m}(\mathbf{r}) = M_\nu \hat{\mathbf{e}}_\nu \quad (16)$$

where  $M_\nu$  is the magnetization and  $\hat{\mathbf{e}}_\nu$  is the magnetization direction. Vector-spin DFT calculations allow to estimate whether Eq. (16) is a good approximation or not (cf. Fig. 2). If the magnetization density in the vicinity of some atom  $\nu$  is expressible by Eq. (16), then the total energy of a magnetic system as a function of its magnetic structure can be described as a functional  $E[\{\hat{\mathbf{e}}_\nu\}]$  of the directions of the magnetic moments at the atoms  $\nu$  in the magnetic unit cell. In this context collinear states ( $\hat{\mathbf{e}}_\nu$  is identical for all atoms) are special solutions where  $E[\{\hat{\mathbf{e}}_\nu\}]$  has a local or global maximum or minimum. Therefore, they constitute an important class of magnetic configurations that are often realized in magnetic materials. Unlike in non-spinpolarized DFT it is, however, in practical calculations not guaranteed that the obtained solution,  $\underline{n}(\mathbf{r})$ , is really the ground state and often several metastable solutions can be obtained.

## 2.1 Spin-dynamics, magnetic torque

If one is interested in the magnetic ground state of a system of given chemical composition and atomic positions, the final goal is to minimize the functional  $E[\{\hat{\mathbf{e}}_\nu\}]$ . The dimensionality of this problem will of course depend on the size of the chosen unit cell (some multiple of the chemical unit cell) and this minimization will involve the tricky task to determine the absolute minimum on a high-dimensional total energy surface. In analogy to molecular dynamics, i.e. the problem of minimizing the energy as a function of the atomic positions, we introduce here a spin dynamics, where the magnetic orientations,  $\hat{\mathbf{e}}_\nu$ , take the role of the variables.

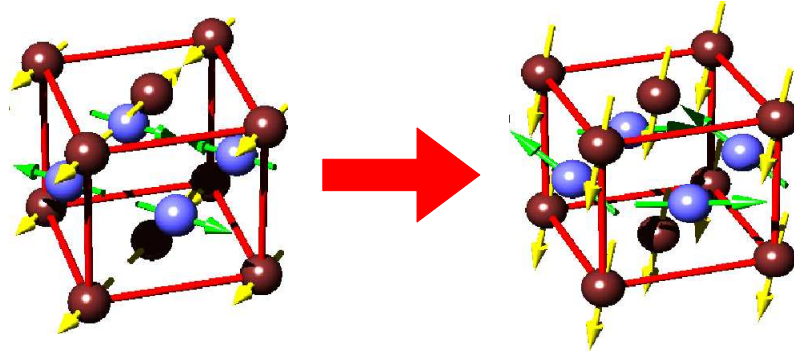


**Fig. 3:** Determination of the magnetic ground state of ordered FeMn: the magnetic structure of the disordered alloy is a 2q-state (left). In an ordered alloy a more complex magnetic arrangement is obtained (right) by “relaxation” of the local spin directions.

Any vector-spin DFT calculation has to start with a reasonably chosen spin configuration in a prescribed unit cell. On a simple level, one can “relax” the directions of the magnetization at the atoms like a relaxation of the atomic structure (e.g. at a surface) is done. The magnetization directions,  $\hat{\mathbf{e}}_\nu$ , will then generally change to minimize the total energy (cf. Fig. 3). The final magnetic state, that will be reached, will in general depend on the starting point of the calculation and a more elaborate technique will be needed to avoid being trapped in some local minimum of  $E[\{\hat{\mathbf{e}}_\nu\}]$ .

To this end we have to develop an equation of motion for the magnetization of an atom. To keep things simple, we will focus on the case, where the magnetization stays collinear within the vicinity of the atom. Let us start from the Hamiltonian of Eq. (6) and assume that the external potential matrix,  $\underline{v}(\mathbf{r})$ , has been chosen to be diagonal and the exchange-correlation potential is separated into diagonal and off-diagonal parts. Following Antropov et al. [18, 19] we set up a time-dependent analogon of Eq. (6):

$$i \frac{d\Phi}{dt} = [H_d - \underline{\sigma} \cdot \mathbf{B}(\mathbf{r}, t)] \Phi \quad \text{where} \quad \Phi = \begin{pmatrix} \phi^{(+)} \\ \phi^{(-)} \end{pmatrix}, \quad (17)$$

and  $H_d$  is the Hamiltonian that contains now only diagonal parts.

We will now separate the evolution of the magnetization into fast (value of the magnetization) and slow (direction of the magnetization) degrees of freedom. The former part will be described quantum-mechanically, while the latter is treated on a semiclassical level. At a given time,  $t$ , the time-independent version of Eq. (17) can be solved for a given magnetization characterized by  $\{\hat{\mathbf{e}}_\nu\}$ . Now we have to determine an equation of motion for the magnetization  $\mathbf{m}(\mathbf{r}, t)$ .

This equation of motion can be obtained by multiplying Eq. (17) from the left with  $\Phi^* \underline{\sigma}$  and adding the complex conjugate equation. Comparing to the time derivative of Eq. (11) and using the relation  $\underline{\sigma}(\underline{\sigma} \cdot \mathbf{B}) = \mathbf{B} - i \underline{\sigma} \times \mathbf{B}$  we get

$$\frac{d\mathbf{m}(\mathbf{r}, t)}{dt} = 2\mathbf{m} \times \mathbf{B} + \frac{i}{2} \nabla(\Phi^* \underline{\sigma} \cdot \nabla \Phi - c.c.). \quad (18)$$

The second term on the right side is complicated and describes longitudinal changes of the magnetization, which we will not consider on this level. Omitting this term, Eq. (18) describes the precession of the magnetization direction at an atom under the influence of the magnetic field generated by the atom itself and other atoms of the crystal.



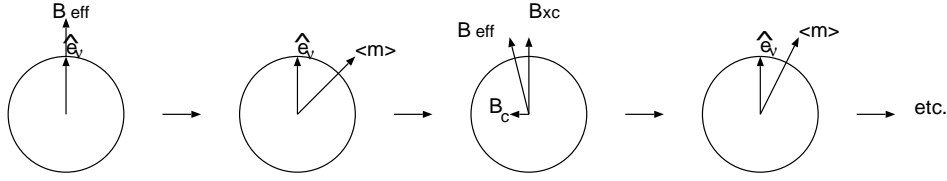


**Fig. 4:** Determination of the constraint field: Initially, the effective  $\mathbf{B}$ -field is parallel to the prescribed direction  $\hat{\mathbf{e}}^\nu$  (left). The resulting magnetization,  $\langle \mathbf{m} \rangle$ , generally is not parallel to this direction. Therefore, a constraint field  $\mathbf{B}_c$  is introduced, that points in opposite direction to the component of the magnetization that is perpendicular to  $\hat{\mathbf{e}}^\nu$ . Using this  $\mathbf{B}_{\text{eff}}$ , the direction of the magnetization is then adjusted towards  $\hat{\mathbf{e}}^\nu$  (right).

Returning once more to Eq. (16), we can simplify Eq. (18) and write for the evolution of the magnetization direction in atom  $\nu$

$$\frac{d\hat{\mathbf{e}}_\nu}{dt} = -\frac{2}{\mu_B} \hat{\mathbf{e}}_\nu \times \mathbf{I}_\nu \quad (19)$$

where  $\mathbf{I}_\nu = \mu_B \mathbf{B}$ . If we explicitly also want to take into account the effect of other fields acting onto a magnetization direction, e.g. stemming from the spin-orbit interaction (magnetic anisotropy) or dipole-dipole interaction, these fields can be added to Eq. (19) into  $\mathbf{I} = \mathbf{I}_\nu + \mathbf{I}_{\text{SO}} + \mathbf{I}_{\text{d-d}}$ . More general expressions of Eq. (19), suitable for spin-dynamics with finite temperatures included, can be found in reference [19].

The next question, that has to be answered, is how to determine the fields  $\mathbf{I}_\nu$ , i.e. given a certain set of magnetization directions  $\{\hat{\mathbf{e}}_\nu\}$  what is the torque on a selected magnetic moment [20]. This problem can be solved in constrained vector-spin density functional theory, as introduced in the next section.

## 2.2 Constrained DFT

In general, an arbitrary magnetic configuration given by a set of local (atomic) magnetization directions  $\{\hat{\mathbf{e}}_\nu\}$  is not an extremum or a stationary solution of the total energy functional  $E[\underline{n}(\mathbf{r})]$ . Exceptions are high symmetry states, like collinear magnetic states, a certain class of spin-spiral states (see Sec. 2.3) and particular linear superpositions of several spin-spiral states. The constrained density functional theory developed by Dederichs *et al.* [21] provides the necessary generalization to deal with arbitrary magnetic configurations, i.e. configurations where the orientations of the local moments are constrained to non-equilibrium directions. We define a generalized energy functional  $\tilde{E}[\underline{n}(\mathbf{r})|\{\hat{\mathbf{e}}_\nu\}]$ , where we ensure that the average magnetization in an atom,  $\langle \mathbf{m} \rangle_\nu$ , points in the direction  $\hat{\mathbf{e}}_\nu$ . This condition,  $\hat{\mathbf{e}}_\nu \times \langle \mathbf{m} \rangle_\nu = 0$ , is introduced by a Lagrange multiplier,  $\lambda$ , so that [22]

$$\begin{aligned} \tilde{E}[\underline{n}(\mathbf{r})|\{\hat{\mathbf{e}}_\nu\}] &= E[\underline{n}(\mathbf{r})] + \sum_\nu \lambda^\nu \cdot (\hat{\mathbf{e}}_\nu \times \langle \mathbf{m} \rangle_\nu) \\ &= E[\underline{n}(\mathbf{r})] + \mu_B \sum_\nu \mathbf{B}_c^\nu \cdot \langle \mathbf{m} \rangle_\nu. \end{aligned} \quad (20)$$

Here, we recast the Lagrange multiplier in the form of a magnetic field,  $\mathbf{B}_c^\nu$ , which is the constraining field in atom  $\nu$  that keeps the local (integrated) magnetic moment, i.e. the magnetiza-

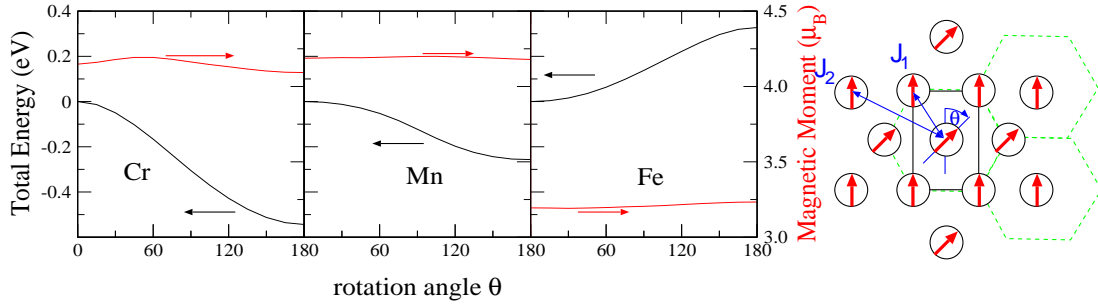


**Fig. 5:** Total energy and magnetic moment of hexagonal monolayers of Cr, Mn, and Fe as a function of the angle of the magnetization in a two-atomic unit cell (right).  $\theta = 0^\circ$  corresponds to a ferromagnetic state,  $\theta = 180^\circ$  is a row-wise antiferromagnetic state. As lattice constant we chose the parameters of the Ag(111) surface. In the schematic picture of the hexagonal monolayer (right) the coupling to nearest neighbors ( $J_1$ ) and next-nearest neighbors ( $J_2$ ) is indicated.

tion density averaged over the sphere where Eq. (16) holds,

$$\langle \mathbf{m}(\mathbf{r}) \rangle_\nu = \mathbf{M}^\nu = \int_{MT^\nu} \mathbf{m}(\mathbf{r}) d^3r, \quad (21)$$

parallel to the prescribed direction  $\hat{\mathbf{e}}_\nu$ .

In an actual constrained local moment (CLM) calculation  $\underline{n}(\mathbf{r})$  and  $\mathbf{B}_c^\nu$  have to be determined self-consistently. The density matrix is calculated in the usual self-consistency cycle. At the same time, the local constraint fields  $\mathbf{B}_c^\nu$  have to be adjusted, until the constraint conditions,  $\hat{\mathbf{e}}_\nu \times \langle \mathbf{m} \rangle_\nu = 0$ , are fulfilled (cf. Fig. 4). At the end of such a calculation we obtain the self-consistent densities and a set of local constraint B-fields. The total energy of the system is given by the constrained energy functional, Eq. (20).

According to the Hellmann-Feynman theorem we find that the change of the energy due to a change in magnetization direction,  $d\hat{\mathbf{e}}_\nu$ , is given by  $dE = -\mu_B \mathbf{M}^\nu \cdot (\mathbf{B}_c^\nu \times d\hat{\mathbf{e}}_\nu)$ . Therefore, the constraint field can be interpreted as a torque acting on the magnetic moment, in the spirit of the spin dynamics, formulated in the previous section. Thus, we have set up a formalism that allows us to find – at least in principle – the magnetic ground state of a system by spin-dynamics [23]. But CLM calculations can also be used in a different way: In the next section we will describe how they can be used to determine the exchange interactions in a system and utilize these results in models, like the classical Heisenberg model, to obtain information about the ground state, but also about excited states of a magnetic system.

## 2.3 Mapping on model Hamiltonians

From the classical Heisenberg model we can derive a Hamiltonian that describes the interaction between two spins  $\mathbf{S}$  at sites  $n$  and  $n'$  in the form

$$H = - \sum_{nn'} J_{nn'} \mathbf{S}_n \cdot \mathbf{S}_{n'} \quad (22)$$

where  $J_{nn'}$  is the exchange coupling constant between the two spins. The sign of  $J_{nn'}$  determines whether a parallel (ferromagnetic) or antiparallel (antiferromagnetic) alignment of  $\mathbf{S}_n$

and  $\mathbf{S}_{n'}$  is preferred. This can be used as a phenomenological starting point in the investigation of the magnetic interaction in a crystal. Although the Heisenberg model was originally introduced for magnetic insulators with localized moments [24], we can also apply Eq. (22) to metallic systems, as shown in Fig. 5. In these hexagonal unsupported monolayers the behavior of the total energy as a function of the relative angle between the atoms can be described as cosine-like function, the exchange coupling constant being negative for Cr and Mn (preferring antiferromagnetic coupling) and positive for Fe (leading to a ferromagnetic ground state). The total energy has been calculated by a constrained DFT calculation as described above. We further see, that the magnetic moment does not change significantly as the spins are rotated, an important requirement for the application of the Heisenberg model.

From the right part of Fig. 5 we can see that rotating the local magnetic moment direction of one atom in the two-atom unit cell of the hexagonal lattice will change the relative orientation of that atom to four nearest neighbors, but does not affect two of the nearest neighbor (NN) atoms. Likewise, only four of the six second-NN atoms will change the relative orientation to the original atom. This leads to an expression for the total energy in the classical Heisenberg model up to second-NN:

$$E = -S^2(J_1 + J_2)(2 + 4 \cos \theta) \quad (23)$$

if  $\mathbf{S}$  is now the total spin moment treated as a classical vector. This means, from a constrained local moment calculation we can at least estimate the size of  $(J_1 + J_2)$ . It is not difficult to find other unit cells and rotations that allow the determination of other linear combinations of  $J_1$  and  $J_2$ , thereby separating the individual exchange coupling constants [25].

Of course, the energies obtained from the CLM calculation contain contributions of all  $J_n$  and also from interactions that are not described by the Heisenberg model. Examples, like the biquadratic interaction or the 4-spin interaction result from hopping processes between four sites, inclusion of spin-orbit interaction gives rise to a third-order process, the so-called Dzyaloshinsky-Moriya interaction [26]. All these different interaction terms can be extracted from a set of suitable *ab-initio* calculations (possibly including spin-orbit interaction) and can be used to determine the magnetic ground state within the chosen model.

### 3 Beyond the ground state

#### 3.1 Low temperatures: magnons and spin waves

In a periodic crystal it is convenient to replace the quantities in Eq. (22) by their Fourier-transformed equivalents:

$$\mathbf{S}(\mathbf{q}) = \frac{1}{N} \sum_n \mathbf{S}_n e^{-i\mathbf{q}\mathbf{R}_n} \quad \text{and} \quad J(\mathbf{q}) = \sum_n J_{0n} e^{-i\mathbf{q}\mathbf{R}_n}. \quad (24)$$

Exploiting the translational invariance of the lattice, we can then rewrite Eq. (22) as

$$H = -N \sum_{\mathbf{q}} J(\mathbf{q}) \mathbf{S}(\mathbf{q}) \cdot \mathbf{S}(-\mathbf{q}) \quad (25)$$

where we have to ensure that the length of all spins  $\mathbf{S}_n^2 = S^2$  is conserved on all sites  $n$ . This condition is fulfilled by solutions of the type [26]

$$\mathbf{S}_n = S (\hat{\mathbf{e}}_x \cos(\mathbf{q} \cdot \mathbf{R}_n) + \hat{\mathbf{e}}_y \sin(\mathbf{q} \cdot \mathbf{R}_n)) \quad (26)$$

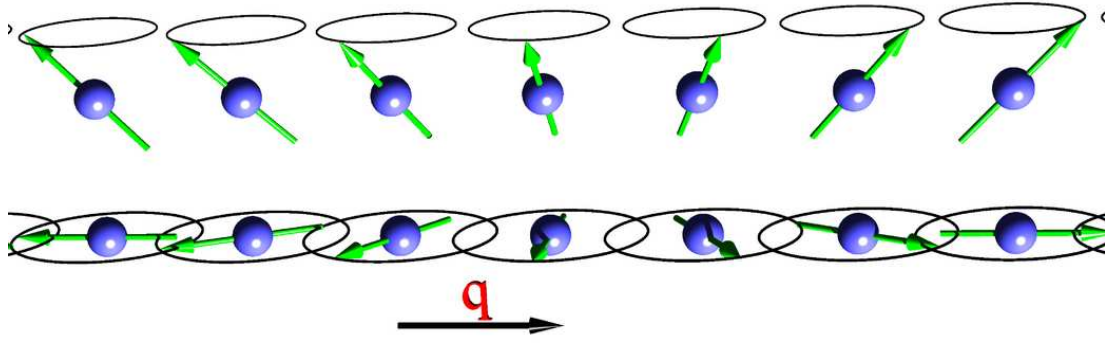


**Fig. 6:** Spiral spin density wave (SSDW) or spin spiral propagating along the  $z$ -axis with a wavevector  $\mathbf{q}$ . The opening angle is  $45^\circ$  in the upper and  $90^\circ$  in the lower example.

where the unit vectors  $\hat{\mathbf{e}}_x$  and  $\hat{\mathbf{e}}_y$  just have to be perpendicular to each other, otherwise their directions are arbitrary. Eq. (26) describes a spiral spin density wave (SSDW) as shown in the lower half of Fig. 6. A more general form of SSDWs can be obtained, when the magnetization precesses on a cone with an opening angle  $\vartheta$ :

$$\mathbf{S}_n = S (\hat{\mathbf{e}}_x \cos(\mathbf{q} \cdot \mathbf{R}_n) \sin \vartheta + \hat{\mathbf{e}}_y \sin(\mathbf{q} \cdot \mathbf{R}_n) \sin \vartheta + \hat{\mathbf{e}}_z \cos \vartheta) \quad (27)$$

as shown in the upper half of Fig. 6.

These SSDWs are general solutions of the Heisenberg model. From Eq. (25) one can conclude that the SSDW with the lowest total energy will be the one with the propagation vector  $\mathbf{Q}$  which maximizes  $J(\mathbf{q})$ . E.g. if  $\mathbf{Q} = 0$  maximizes  $J(\mathbf{q})$ , the solution corresponds to the ferromagnetic state, if  $\mathbf{Q} = \hat{\mathbf{e}}_z \frac{\pi}{a_z}$  and  $a_z$  is the lattice constant in  $z$ -direction, then the structure is layered antiferromagnetic in  $z$ -direction. Some other examples – for a hexagonal monolayer – are illustrated in figure 7.

SSDWs are sometimes also called frozen magnons, since a spin-spiral looks like a “snap shot” of a single magnon at a fixed time. Spin-spiral calculations can therefore be used to simulate the effect of temperature on a magnetic system in the adiabatic approximation, in particular at very low temperatures, when magnons with long wavelength dominate. But also at  $T = 0$  many compounds and even elements show SSDW ground states. Some examples were shown in Fig. 1.

At low, but finite temperatures, collective spin-wave excitations or magnons are excited in the ferromagnetic crystal. These magnons can again be characterized by their wave-vector  $\mathbf{q}$ . In the long wavelength limit, i.e. around  $\mathbf{q} = 0$  the spin-wave dispersion behaves almost quadratically and can be described as  $Dq^2$ . The spin stiffness,  $D$ , characterizes the magnetic properties of a ferromagnet at low temperatures and can also be calculated from the exchange coupling constants:

$$D = \frac{2}{3M} \sum_n J_{0n} R_{0n}^2. \quad (28)$$

Here,  $M$  is the magnetic moment of the ferromagnetic state. Some results of *ab-initio* calculations are given in table 2. For Fe and Co agreement with experimental data is reasonable, but for Ni most methods fail to reproduce the experimental spin stiffness.

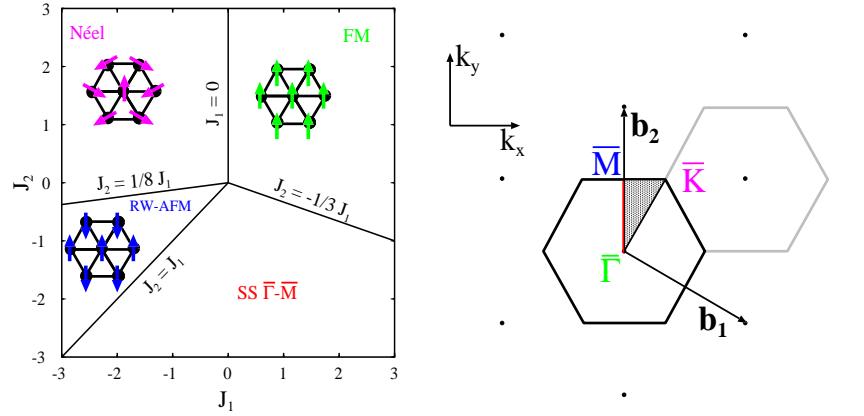


**Fig. 7:** Phase diagram of the hexagonal lattice in next-nearest neighbor approximation of the classical Heisenberg model: two collinear, a ferromagnetic (FM) and a row-wise antiferromagnetic (RW-AFM) solution can be obtained, and two non-collinear solutions, the Néel-state and a SSDW with  $\mathbf{q}$ -vectors along the line  $\bar{\Gamma} - \bar{M}$  of the Brillouin zone (right). The FM, RW-AFM and Néel-state correspond to SSDWs with  $\mathbf{q}$ -vectors on the high-symmetry points  $\bar{\Gamma}$ ,  $\bar{M}$  and  $\bar{K}$ , respectively.

**Table 2:** Calculated and experimental spin-wave stiffness ( $D$ ) for Fe, Co and Ni. The theoretical data was obtained in different approximations as described by Rosengard and Johansson [28] [th.(1)], Shallcross and coworkers [7] [th.(2)] and Padjar et al. [27] [th.(3)], experimental data was taken as cited in these references.

	D (meV Å <sup>2</sup> )			
	th.(1)	th.(2)	th.(3)	exp.
Fe (bcc)	247	322, 313	250	280, 314, 330
Co (fcc)	502	480, 520	663	510, 580
Ni (fcc)	739	541, 1796	756	422, 550, 555

### 3.2 Spin-spirals and the generalized Bloch theorem

A very elegant treatment of spin-spirals by first-principle calculations is possible when the generalized Bloch theorem [29, 30] is applied. However, this theorem can only be proven, when spin-orbit coupling is neglected. For this reason the spin-rotation axis will always be considered as parallel to the  $z$ -axis of the spin coordinate-frame. Thus, only the  $m_x$  and  $m_y$  components are rotated, while  $m_z$  does not change. Following Sandratskii [30] we can define a generalized translation,  $\mathcal{T}_n$ , that combines a lattice translation,  $\mathbf{R}_n$ , and a spin rotation  $\mathbf{U}$  that commutes with the Hamiltonian  $H$ . Applying such a generalized translation to  $H\Phi$  yields

$$\begin{aligned}
 \mathcal{T}_n H(\mathbf{r})\Phi(\mathbf{r}) &= \mathbf{U}(-\mathbf{q}\mathbf{R}_n)H(\mathbf{r} + \mathbf{R}_n)\mathbf{U}^\dagger(-\mathbf{q}\mathbf{R}_n)\mathbf{U}(-\mathbf{q}\mathbf{R}_n)\Phi(\mathbf{r} + \mathbf{R}_n) \\
 &= H(\mathbf{r})\mathbf{U}(-\mathbf{q}\mathbf{R}_n)\Phi(\mathbf{r} + \mathbf{R}_n)
 \end{aligned}
 \tag{29}$$

where  $U(\mathbf{q}\mathbf{R}_n)$  is the spin 1/2 rotation matrix

$$U(\mathbf{q}\mathbf{R}_n) = \begin{pmatrix} e^{-i\varphi/2} & 0 \\ 0 & e^{i\varphi/2} \end{pmatrix}, \quad \varphi = \mathbf{q} \cdot \mathbf{R}_n. \quad (30)$$

In analogy with the proof of Bloch's theorem [31] it follows that the eigenstates can be chosen such that

$$\mathcal{T}_n \Phi(\mathbf{k}, \mathbf{r}) = U(-\mathbf{q}\mathbf{R}_n) \Phi(\mathbf{k}, \mathbf{r} + \mathbf{R}_n) = e^{i\mathbf{k} \cdot \mathbf{R}_n} \Phi(\mathbf{k}, \mathbf{r}). \quad (31)$$

Since these eigenstates are labeled with the same Bloch vector  $\mathbf{k}$  as the eigenstates of the translation operator without the spin rotation, the lattice periodic part of these states follows the chemical lattice,  $\mathbf{R}_n$ , i.e. we can calculate the spin spiral state in the chemical unit cell. In a reciprocal-space method, i.e. when all quantities like potential or wavefunctions are expressed as Fourier-transforms, the computational effort scales with the size of the unit cell. Without the application of the generalized Bloch theorem the investigation of spin spiral states requires very large unit cells, and a description of SSDWs that are incommensurate with the lattice would be not possible.

Since the spin-spiral is the exact solution of the classical Heisenberg model at  $T = 0$ , it is believed that they cover a large and important part of the phase space of possible spin states. Thus among all possible magnetic states, spin-spirals are the next relevant class of spin states besides the high-symmetry magnetic states, i.e. the ferromagnetic, antiferromagnetic, or ferrimagnetic configurations.

A further computational simplification can be reached, when the SSDW is considered just as a small perturbation to the parent (most often ferromagnetic) structure. This may be justified in the limit of small  $\mathbf{q}$ -vectors or small opening angles  $\vartheta$  (cf. Eq. (27)). The limit of  $\vartheta \rightarrow 0$  is particularly important in the study of finite temperature effects, since it describes elementary perturbations of the collinear ground state. In this limit again the magnetic force theorem [17] can be applied, thus reducing the computational efforts significantly [32].

In real-space methods the calculation of  $J(\mathbf{q})$  is most conveniently done via the right of Eq. (24), i.e. the evaluation of  $J_{0n}$ . In this case the direction of the magnetization at a reference atom, 0, is perturbed and the response on the other atoms,  $n$ , calculated. Also in this case a kind of magnetic force theorem can be used [5].

### 3.3 High temperatures: $T_C$ and $T_N$

Let us now see, how higher temperatures will influence the magnetic order in a ferromagnetic solid. Staying within the Heisenberg model, we will assume that the magnitude of the magnetic moments at the atoms will – in first approximation – not be changed, and discuss just their mutual orientation. At  $T = 0$  the spin at a selected atom will be fixed in parallel direction to the spins at all other atoms by an effective field that will be proportional to  $S \sum_n J_{0n} = S J_0$ . At a finite temperature  $T$ , this field, that acts on the spin at site 0 is reduced due to the thermal fluctuation on the sites  $n$ . The thermal average of the projection of the spin at site  $n$  on the spin at site 0 is denoted as  $\langle S(\mathbf{R}_n) \rangle$ . In the “mean field approximation” (MFA), it is assumed that the effective field at finite temperatures that acts on spin 0 is:

$$B_{\text{eff}} = \sum_n J_{0n} \langle S(\mathbf{R}_n) \rangle \quad (32)$$

In this model it is possible to calculate the temperature-dependence of the average magnetization of the solid and, specifically, the temperature where the average magnetization vanishes, the

critical temperature. For a ferromagnet this temperature is called Curie temperature and in the MFA it is given by

$$T_C = \frac{2S(S+1)}{3k_B} J_0 \quad (33)$$

It has to be mentioned, that in most cases the MFA severely overestimates  $T_C$  (by about 20 to 50%, depending on the lattice). Nevertheless, it gives a simple estimate of the ordering temperature in systems, where the approximations of the Heisenberg model are reasonable. On the other hand, some properties, like the – material independent – critical exponents, are in any case not usefully reproduced by the MFA.

On a more sophisticated level, the “random phase approximation” (RPA) can give quite reliable results. In contrast to the MFA, where the thermal averaging was done over the sites  $n$  that determine  $B_{\text{eff}}$ , here the Hamiltonian is first transformed into reciprocal space (Eq. (25)), and then the averaging is done over one of the Fourier components:

$$H = -N \sum_{\mathbf{q}} J(\mathbf{q}) \mathbf{S}(\mathbf{q}) \cdot \langle \mathbf{S}(-\mathbf{q}) \rangle \quad (34)$$

If the term  $S(S+1)$  is included in the exchange coupling constants (as it is usually done, when the  $J$ ’s are determined from first-principles calculations), then the Curie temperature in the MFA and RPA can be expressed as

$$k_B T_C^{\text{MFA}} = \frac{2}{3} J_0 \quad k_B T_C^{\text{RPA}} = \frac{2}{3} \left( \sum_{\mathbf{q}} \frac{1}{J(\mathbf{q})} \right)^{-1} \quad (35)$$

From these expressions it is obvious, that calculating  $T_C$  in the RPA involves not more information than what is needed on a mean-field level, if the exchange coupling constants are calculated in reciprocal space by using the generalized Bloch theorem.

Also for antiferromagnets (or, generally spin-spiral states characterized by a vector  $\mathbf{Q}$ ) expressions for the ordering temperature, the Néel temperature  $T_N$ , can be derived. In the MFA with  $S(S+1)$  again included in  $J$ , this is given simply by

$$k_B T_N^{\text{MFA}} = \frac{2}{3} J(\mathbf{Q}) \quad (36)$$

while a slightly more involved expression can be derived in the random phase approximation [5]. Comparison of these results with experimental values gave reasonable results, e.g. for bcc europium Néel temperatures of 147 K and 110 K were obtained in MFA and RPA, respectively [5]. These values have to be compared to the experimental  $T_N$  of  $90.5 \pm 0.5$  K.

Although there exist several more methods to calculate critical temperatures from DFT results, we will outline here just one further possibility, which seems to be rather flexible and appropriate for many systems with different magnetic ground states: the Monte Carlo technique (MC) allows to study finite-temperature magnetic properties by implementation of a Heisenberg Hamiltonian (Eq. (22), possible with extensions like biquadratic terms or an uniaxial anisotropy (see below)), into a Metropolis algorithm [33]. Unit cells of different size are then studied so that finite-size effects can be eliminated. In these unit cells the evolution of the magnetic property in question (in our case the average magnetization) as a function of temperature can then be monitored.

**Table 3:** Calculated and experimental Curie temperature  $T_C$  for some ferromagnetic materials. MFA and RPA data for Fe, Co and Ni taken from Padjar et al. [27], MFA2 results and experimental values as quoted by Shallcross and coworkers [7], while the MC results were obtained by Rosengaard and Johansson [28]. Data for Gd can be found in the papers of Kurz et al. [8] and Turek and coworkers [34].

	$T_C$ (K)				
	MFA	MFA2	RPA	MC	exp.
Fe (bcc)	1414	550, 1190	950	1060	1044 – 1045
Co (fcc)	1645	1120, 1350	1311	1080	1388 – 1390
Ni (fcc)	397	320, 820	350	510	624 – 631
Gd (hcp)	334				293

Results of *ab-initio* calculations of the Curie temperature of Fe, Co and Ni are presented in table 3. From this table one can easily see that, compared to RPA, the MFA typically overestimates  $T_C$  by 25–50%. For Fe and Co RPA gives quite good estimates of the Curie temperature, while for Ni  $T_C$  is underestimated in both approximations. MC simulations work better for Ni and Fe, but give a too low  $T_C$  for Co.

While we quoted here results for “simple” metals, it is nowadays possible to investigate in the same manner the temperature dependent properties of complex multicomponent systems, e.g. half-metallic Heusler alloys [35] or dilute magnetic semiconductors [36]. In this way, materials for modern spintronic applications can be studied at physically relevant temperatures and their detailed magnetic properties can be predicted on the basis of quantum-mechanics. The combination of advanced numerical techniques and massively parallel supercomputers makes computational material science one of the most rapidly growing fields of physics with relevance for basic and applied science.



## References

- [1] P. Hohenberg and W. Kohn, Phys. Rev. **136**, B864 (1964)
- [2] W. Kohn and L. J. Sham, Phys. Rev. **140**, A1133 (1965)
- [3] U. von Barth and L. Hedin, J. Phys. C: Solid State Phys. **5**, 1629 (1972)
- [4] S. Di Napoli, A. M. Llois, G. Bihlmayer, S. Blügel, M. Alouani, and H. Dreysse, Phys. Rev. B **70** 174418 (2004)
- [5] I. Turek, J. Kudrnovský, M. Diviš, P. Franek, G. Bihlmayer, and S. Blügel, Phys. Rev. B **68**, 224431 (2003)
- [6] V. L. Moruzzi, J. F. Janak, and A. R. Williams, *Calculated Electronic Properties of Metals*, (Pergamon, New York, 1978)
- [7] S. Shallcross, A. E. Kissavos, V. Meded, and A. V. Ruban, Phys. Rev. B **72**, 104437 (2005)
- [8] Ph. Kurz, G. Bihlmayer, and S. Blügel, J. Phys.: Condens. Matter **14**, 6353 (2002)
- [9] H. W. White, B. J. Beaudry, P. Burgardt, S. Legvold, and B. N. Harmon, AIP Conf. Proc. **29**, 329 (1975)
- [10] D. J. Singh and J. Ashkenazi, Phys. Rev. B **46**, 11570 (1992)
- [11] G. Vignale and M. Rasolt, Phys. Rev. B **37**, 10685 (1988)
- [12] H. A. Bethe and E. E. Salpeter *Quantum Mechanics of One- and Two-Electron Systems* (New York, Plenum 1977)
- [13] T. Thonhauser, D. Ceresoli, D. Vanderbilt, and R. Resta, Phys. Rev. Lett. **95**, 137205 (2005)
- [14] I. Yang, S. Y. Savrasov, and G. Kotliar, Phys. Rev. Lett. **87**, 216405 (2001)
- [15] J. Stöhr, J. Magn. Magn. Mater. **200**, 470 (1999)
- [16] G. Bihlmayer in: *Magnetism goes Nano, Schriften des FZ-Jülich: Matter and Materials* (26) (Jülich, 2005)
- [17] M. Weinert, R. E. Watson, and J. W. Davenport, Phys. Rev. B **32**, 2115 (1985)
- [18] V. P. Antropov, M. I. Katsnelson, M. van Schilfgaarde, and B. N. Harmon, Phys. Rev. Lett. **75**, 729 (1995)
- [19] V. P. Antropov, M. I. Katsnelson, B. N. Harmon, M. van Schilfgaarde, and D. Kusnezov, Phys. Rev. B **54**, 1019 (1996)
- [20] G. M. Stocks, B. Újfalussy, X.-D. Wang, Y. Wang, D. M. C. Nicholson, W. A. Shelton, A. Canning, and B. L. Györffy, Phil. Mag. B **78**, 665 (1998)
- [21] P. H. Dederichs, S. Blügel, R. Zeller, and H. Akai, Phys. Rev. Lett. **53**, 2512 (1984)

- [22] Ph. Kurz, F. Förster, L. Nordström, G. Bihlmayer, and S. Blügel, *Phys. Rev. B* **69**, 024415 (2004)
- [23] B. Újfalussy, X.-D. Wang, D. M. C. Nicholson, W. A. Shelton, G. M. Stocks, Y. Wang, and B. L. Györffy, *J. Appl. Phys.* **85**, 4824 (1999)
- [24] P. W. Anderson, *Theory of Magnetic Exchange Interactions: Exchange in Insulators and Semiconductors*, *Solid State Physics* **14**, 99 (1963)
- [25] Ph. Kurz, G. Bihlmayer, K. Hirai, and S. Blügel, *Phys. Rev. Lett.* **86**, 1106 (2001)
- [26] K. Yosida, *Theory of Magnetism* (Springer, Berlin-Heidelberg, 1996)
- [27] M. Pajda, J. Kudrnovský, I. Turek, V. Drchal, and P. Bruno, *Phys. Rev. B* **64**, 174402 (2001)
- [28] N. M. Rosengaard and Börje Johansson, *Phys. Rev. B* **55**, 14975 (1997)
- [29] C. Herring, in *Magnetism*, (Ed. G. Rado and H. Suhl) (Academic, New York, 1966)
- [30] L. M. Sandratskii, *Phys. Status Solidi B* **136**, 167 (1986)
- [31] N. Ashcroft and N. Mermin, *Solid State Physics* (Saunders College, Philadelphia, 1976)
- [32] M. Ležaić, PhD Thesis, Jülich (2005)
- [33] N. Metropolis, A. W. Rosenbluth, M. N. Rosenbluth, A. H. Teller, and E. Teller, *J. Chem. Phys.* **21**, 1087 (1953)
- [34] I. Turek, J. Kudrnovský, G. Bihlmayer, and S. Blügel, *J. Phys.: Condens. Matter* **15**, 2771 (2003)
- [35] E. Şaşıoğlu, L. M. Sandratskii, and P. Bruno, *J. Appl. Phys.* **98**, 063523 (2005)
- [36] K. Sato, P. H. Dederichs, and H. Katayama-Yoshida, *J. Supercond.* **18**, 33 (2005)